

ASSESSING THE EFFECT OF ALOS-2 DATA UTILIZATION ON THE ACCURACY OF ESTIMATION VERTICAL AND HORIZONTAL DEFORMATION COMPONENTS IN THE AREA OF HARD COAL MINING EXPLOITATION IN POLAND BY USING DIFFERENTIAL SYNTHETIC APERTURE RADAR INTERFEROMETRY

K.Pawluszek-Filipiak¹, N. Wielgocka¹, D. Tondaś¹, A. Borkowski⁺,

¹ Institute of Geodesy and Geoinformatics, Wrocław University of Environmental and Life Sciences, Wrocław, Poland
(kamila.pawluszek-filipiak,natalia.wielgocka,damian.tondas@upwr.edu.pl);

Commission III, WG III/3

KEY WORDS: DInSAR, mining subsidence, monitoring, Sentinel-1, ALOS-2, radar interferometry

ABSTRACT:

Mining-induced deformations are characterized by high deformation rates. These deformations consist of both vertical and horizontal components, which should not be neglected during the monitoring of such areas. Unfortunately, Differential Satellite Synthetic Aperture Radar Interferometry (DInSAR) can only measure deformations in the line of sight (LOS) direction towards the satellite. Combining data from ascending and descending geometry allows reconstruction of the vertical and east-west deformation components. Theoretically, at least information from one ascending and one descending geometry is enough to reconstruct the vertical and east-west deformation components; however, for the area of interest three various Sentinel-1 datasets (one ascending and two descending) are available and have been used in the study. Furthermore, considering the availability of other SAR missions with slightly different geometries, the objective of this study was to evaluate the effect of ALOS-2 use on the accuracy of estimating the east-west and vertical cumulative deformation component estimated for a time span of approximately one year. Unfortunately, we have access to only five ALOS-2 scenes within the area of interest. However, the comparison of the decomposed results with GNSS measurements shows that the application of additional ALOS-2 data, even five scenes, allows the root mean square error (RMSE) to be decreased for the vertical and horizontal deformation component from 0.038m to 0.032m and from 0.031m to 0.018m, respectively. This means that the application of ALOS-2 data has a positive value on the accuracy of decomposed vertical and horizontal deformation components.

1. INTRODUCTION

Mining exploitation causes significant ground surface deformations that affect buildings and artificial facilities. Therefore, the measurement and monitoring of these areas are crucial to improve safety, productivity, and costs (Mutke et al., 2019). In Poland, the area of extensive mining exploitation is located in southern Poland and is called the Upper Silesian Coal Basin (USCB), where hard coal is excavated underground. In these areas, the most popular technique is longwall exploitation (Ilieva et al., 2019). Currently, measurements of ground stability are widely carried out by conventional geodetic techniques such as Global Navigation Satellite Systems (GNSS), leveling, or total station which are point-based and therefore do not provide complete information about the spatial deformation pattern of specific phenomena (Pawluszek-Filipiak et al., 2021). Therefore, the opportunities offered by Differential Interferometric Synthetic Aperture Radar (DInSAR) open new ways to study ground surface deformation (Crosetto et al., 2016). However, mining-induced deformations are characterized by a high deformation gradient and non-linearity that very often cause challenges in the proper estimation of deformation rate using DInSAR. Mining deformations consist of vertical and horizontal (east-west and north-south) components, which should not be neglected and are recently a research interest of many scientists (Wang et al., 2018; Yang et al., 2018; Pawluszek-Filipiak and Borkowski 2021). Unfortunately, DInSAR can only measure deformations in the line of sight (LOS) direction towards the satellite. Additionally, due to the near-polar orbit of many SAR missions, estimation of the north-south deformation component

is challenging and even impossible solely. Therefore, usually, a combination of the ascending and descending geometry and assumption that the north component is equal to zero allows one to estimate vertical and east-west deformation components (two unknowns and two equations) (Hanssen, 2001). Nevertheless, increasing the number of SAR satellite observations with various geometrical settings allows one to enhance the geometrical constraints for vertical and horizontal deformation component estimation (Zhang et al., 2020). However, most SAR satellites are almost polar orbiting, thus geometrical constraints in the north-south direction are very weak and therefore the north component is very challenging to estimate. However, the application of other SAR geometries and deformation decomposition using least squares estimation theoretically can help increase the accuracy of the vertical and east-west estimated components. To increase the number of observations, it is helpful to use data from several viewing geometries (Fuhrmann and Garthwaite, 2019). Using data from different SAR sensors will additionally provide increased geometric variation in the images and, depending on the used wavelength, other characteristics of the captured image (Pepe et al., 2012). Sun et al. (2016) used ALOS ascending and ENVISAT descending tracks for LOS decomposition in the area of Zhouqu slow-moving landslides. By adding a dataset from Uninhabited Aerial Vehicle SAR (UAVSAR) to the decomposition, the estimation of the north component is made possible (Wnuk et al., 2021).

Therefore, in this study, we used three SAR geometries determined by Sentinel-1 data (one ascending and two descending) and ALOS-2 data from ascending geometry. Since the ALOS-2 data have been provided by JAXA within the 6th

⁺ This work has been carried out with the collaboration of Professor Andrzej Borkowski who passed away on March 13, 2021, therefore this paper is dedicated to his memory

Research Agreement, only five scenes have been available within the investigated time span. Since the ALOS-2 mission is L-band, the coherence between these images was still good and application of the DInSAR technique was possible. This work is a continuation of our previous study presented in Pawluszek-Filipiak and Borkowski (2020), where we investigated pros and cons of persistent scattered interferometry technique (PSI) proposed by Ferretti et al., 2000; 2001, and DInSAR. Since PSI was unable to estimate the maximum deformation in the center of the subsidence basins and this information is one of the most important information from the mining perspective, we continue our work with the utilization of the DInSAR approach and integration of additional datasets from different SAR missions.

2. STUDY AREA AND DATA USED

2.1 Area of Interest

The Rydułtowy mine is the oldest active mine in the Upper Silesian Coal Basin (USCB) in Poland. The USCB is one of the largest hard coal mining areas in Europe. The Rydułtowy mine is located in the southwest part of the USCB (Figure 1) and covers approximately 46 km². The average daily production of the mine ranges between 9,000 and 9,500 t/day and the extraction depth reaches 800 - 1200 m. This area was investigated during the EPOS-PL project, which allowed the purchase of five passive corner reflectors (CRs) and placed them in the area of interest. EPOS-PL is the Polish implementation of the European Plate Observing System (EPOS) initiative, which aims at the integration of existing and newly created research infrastructures to facilitate the use of multidisciplinary data and products in the field of Earth sciences in Europe.

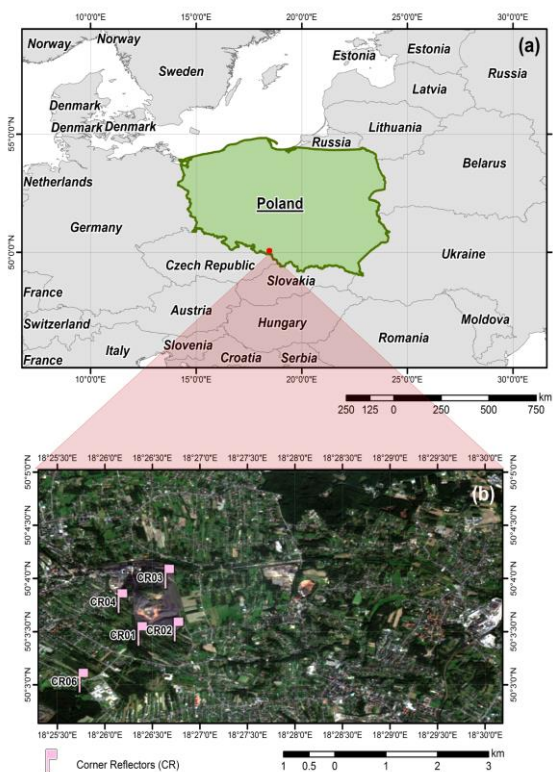


Figure 1. Location of the area of interest on the Europe country map (a) and Rydułtowy mine with CRs based on satellite imagery (b)

2.2 SAR data

Table 1. Specification of the SAR data

Dataset	Sentinel-1A/B	Sentinel-1A/B	Sentinel-1A/B	ALOS-2
orbit mode	ascending	descending	descending	ascending
track	175	51	124	192
incidence angle [°]	38.16	44.06	35.57	31.75
azimuth [°]	81.7	-78.9	-77.4	80.8
no. of images	62	61	62	5
time span	2018/06/28-2019/07/05	2018/06/26-2019/07/09	2018/06/25-2019/07/14	2018/05/19-2019/06/15

To estimate the deformation caused by the coal excavation in Rydułtowy mine, Sentinel-1 as well as ALOS-2 datasets have been used. In this study, we used 62 ascending Sentinel-1 images and 62 and 61 Sentinel-1 images from two descending geometries. Additionally, we used five SAR scenes acquired from ALOS-2 data in the framework of the 6th Research Agreement with the Japan Aerospace Centre (JAXA). More specific information about used datasets is presented in Table 1.

2.3 Ground truth data

In the area of the Rydułtowy mine, five passive CRs have been placed in the framework of the EPOS-PL project. These five CRs were measured using static GNSS observation, where three independent measurement sessions were carried out over three days. More specifically, in the first measurement campaign, the first, second, and third GNSS measurement sessions were carried out on the 2nd, 3rd, and 4th of July 2018, and each session involved at least 10 hours of static GNSS observations. The same processes were repeated for the second measurement campaign carried out between 28th and 30th June 2019. GNSS post-processing calculations were performed using Leica Infinity software, based on precise satellite orbit and clock corrections - CODE final (Dach et al., 2018). The coordinates of the CRs were determined by estimating independent vectors assigned to four reference stations: KATO, TAR1, WOD1, and ZYWI. The reference GNSS stations belonged to the Polish European Position Determination System (EUPOS) network, known as ASG-EUPOS (www.asgeupos.pl). The results of the post-processing calculations were obtained using an ETRF2000 reference frame. Table 2 presents horizontal and vertical deformation estimated from GNSS field measurements.

Table 2. Estimated deformation from GNSS measurement in vertical and horizontal direction

CR No.	GNSS [m]		
	North-South	East-West	Up
CR01	-0.056	-0.125	-0.457
CR02	-0.019	0.079	-0.216
CR03	-0.003	0.019	-0.050
CR04	-0.002	0.030	-0.020
CR06	-0.007	0.026	-0.015

3. METHODOLOGY

Four different SAR datasets have been processed using the consecutive DInSAR approach with minimal possible temporal baseline (usually 6 days for Sentinel-1A/B data). For DInSAR processing, the SARscape® software was used. The minimum cost flow function was used for phase unwrapping and the ALOS-World-3D Digital Elevation Model was used for the removal of the topographic interferometric components. Some bad interferograms were omitted due to the low coherence. Especially, low coherence was observed at CRs during the winter season due to the high snow cover. In this cases, interferograms were calculated based on 12-days revisiting time. Using calculated consecutive interferograms, time-series deformation maps were created and subsequently, the Line-of-Sight (LOS) cumulative deformations were delivered from four various SAR datasets. Additionally, due to the time shift between the acquisition of various SAR scenes, interpolation in time was necessary. Afterwards, cumulative deformation estimated for the same time span from four datasets were used for the decomposition, which has been performed to provide vertical and horizontal components according to equation (1):

$$d_{LOS} = d_u \cos(\theta_{inc}) - \sin \sin(\theta_{inc}) \left[d_n \cos \cos\left(\alpha_h - \frac{3\pi}{2}\right) + d_e \sin \sin\left(\alpha_h - \frac{3\pi}{2}\right) \right] \quad (1)$$

Where: d_{LOS} is the deformation along the LOS direction, α_h is the heading (azimuth) angle, and θ_{inc} is the incidence angle.

Considering that Sentinel-1A/B and ALOS-2 missions have almost polar orbiting satellites and therefore are insensitive to the nothing deformation component, we assumed this component to be equal to 0. This assumption is widely implemented in the literature (Gernhardt and Bamler, 2012, Samsonov et al., 2020; Pawluszek-Filipiak and Borkowski, 2021). Subsequently, east-west and vertical deformation components (d_u, d_e) were estimated by means of the Least Squares Fitting (LSF) according to equation (2):

$$v = Ax - L \quad (2)$$

where:

- v - vector of corrections for observation,
- A - matrix of coefficients with unknowns,
- x - vector of unknowns,
- L - observation vector.

Deformation decomposition was performed in two variants. First variant was based on Sentinel-1 data only (one ascending and two descending geometries) and the second variant was based on integrated Sentinel-1 and ALOS-2 data (two ascending and two descending geometries). The results have been later compared with ground truth data using Root Mean Square Error (RMSE) as presented in equation (3):

$$RMSE_{E,U} = \sqrt{\frac{1}{P} \sum_{i=1}^P (d_{GNSS} - d_{DInSAR})^2} \quad (3)$$

where:

$GNSS$ is the GNSS geodetic reference measurements carried out at the five CRs in the east (E) and vertical (U) direction, respectively

$DInSAR$ may be either the DInSAR east-west or vertical deformation results

P is the number of validated observations-five CRs.

The overall workflow of applied methodology is presented in Figure 2.

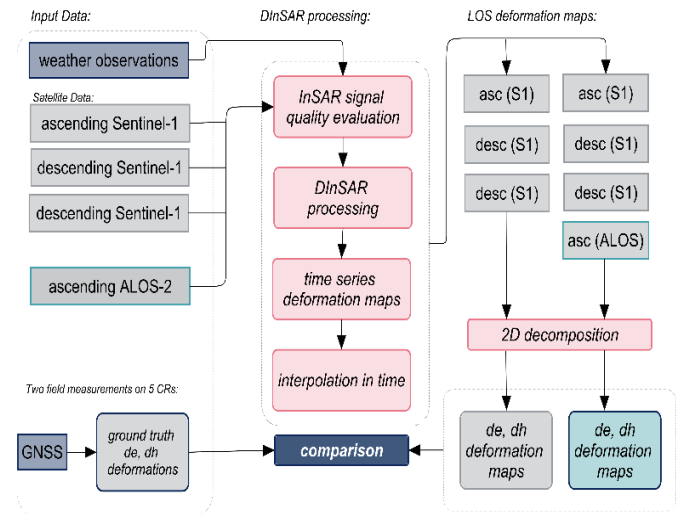


Figure 2. The overall methodology of the presented study

4. RESULTS

4.1 LOS estimated land deformation

Based on the cumulative DInSAR approach from Sentinel-1A/B and ALOS-2 data, four various deformation maps in LOS direction have been captured which are presented in Figure 3 and Figure 4. Figure 3 presents results acquired from descending orbits with no. 51 (Fig. 3a) and no. 124 (Fig. 3b), while Figure 4 presents results from Sentinel-1A/B ascending geometry (Fig. 4a) and ALOS-2 geometry (Fig. 4b). As can be observed, similar results are demonstrated for each orbit, however, slightly bigger deformation gradient can be observed for results from Sentinel-1A/B descending geometry with relative orbit no. 124 and ALOS-ascending dataset. Also a small shift between detected subsidence basins can be observed between ascending and descending geometries, which indicates that there are significant horizontal movements in the investigated study area. Additionally, it can be observed that less pixels with NoData are captured in the results of ALOS-2 data, mostly due to the longer wavelength of L-band sensors with comparison to the C-band of Sentinel-1 and therefore, better coherence. Moreover, it can be observed that the accuracy of ALOS-2 is worse since more yellow color is observed in Figure 4b. This is due to the greater sensitivity of L-band sensors on atmospheric artefacts and therefore smaller measurement accuracy.

4.2 Vertical and horizontal deformation

Figure 5a represents the vertical deformation component estimated from Sentinel-1A/B data only and Figure 5b represents the integrated results from Sentinel-1&ALOS-2. The easting deformation component is shown as a raster and arrows in Figure 6a-b. Similarly, Figure 6a represents the east-west deformation

component estimated from only the Sentinel-1A/B based solution while Figure 6b represents results for the Sentinel-1A/B and ALOS-2 integrated approach. In Figures 5a and 5b no significant differences can be observed. In case of horizontal movements, it can be observed that less bluish colors are present on Figure 6b, which indicated horizontal movement towards the west direction.

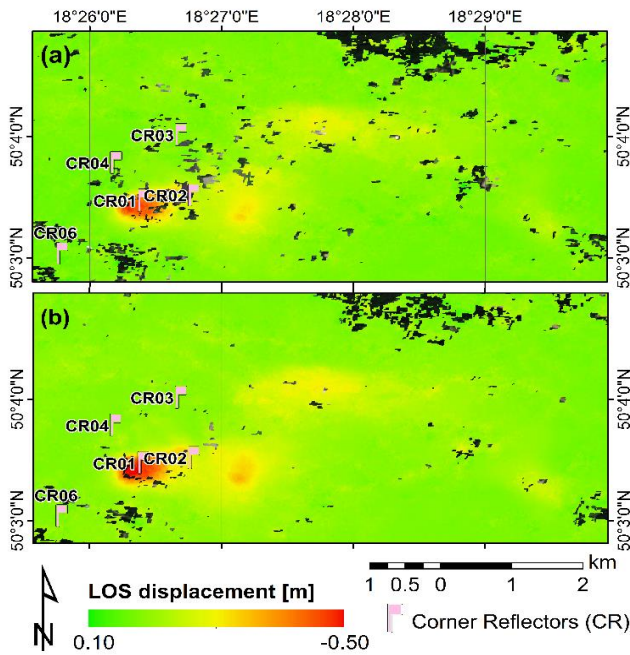


Figure 3. Cumulative deformation of the DInSAR descending orbit with relative number 51 (a) and with relative number 124 (b)

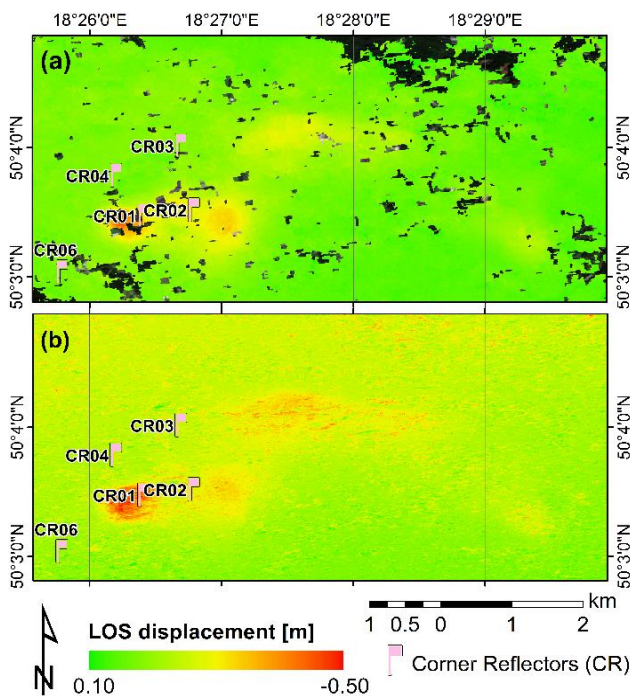


Figure 4. Cumulative deformation of the DInSAR for Sentinel 1A/B ascending orbit with relative number 175 (a) and for ALOS-2 ascending data (b)

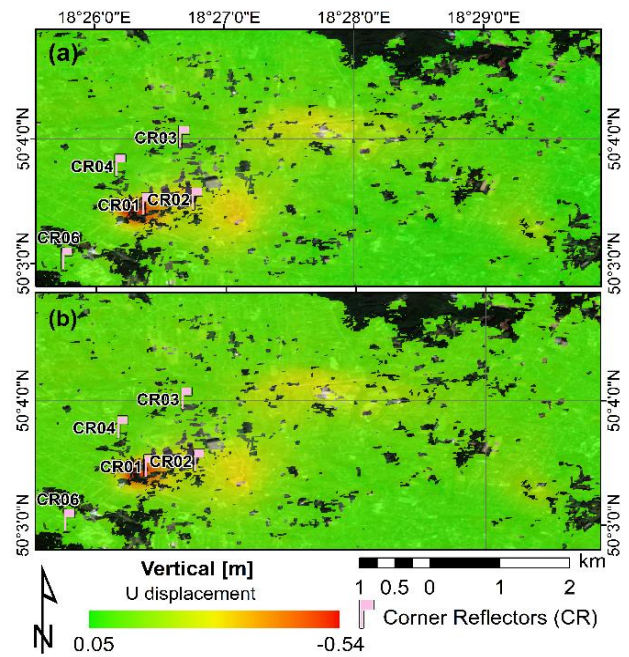


Figure 5. Cumulative vertical deformation from DInSAR estimated for Sentinel-1 data only (a) and for Sentinel-1 and ALOS-2 (b)

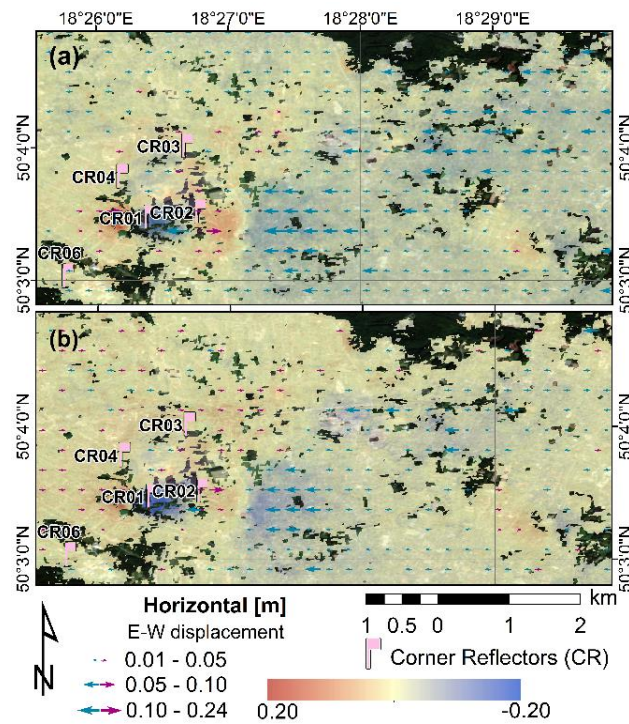


Figure 6. Cumulative horizontal deformation from DInSAR estimated for Sentinel-1 data only (a) and for Sentinel-1 and ALOS-2 (b)

5. ACCURACY ASSESSMENT

Comparison between DInSAR-based deformation components and ground truth data from leveling and GNSS allows evaluating the accuracy of the estimated deformations. The root mean square error (RMSE) (Table 3) has been calculated based on the deviations between the ground truth and the deformation components estimated using Sentinel-1A/B only and the Sentinel-1A/B and ALOS-2 approaches. As can be observed in Table 3, integrated approach with Sentinel-1A/B and ALOS-2 allows us to achieve more accurate results.

Table 3. RMSE for vertical and horizontal deformation estimated by using two decomposition variants

Deformation component	RMSE [m]	
	Sentinel-1A/B	Sentinel-1&ALOS
vertical	0.038	0.032
east-west	0.031	0.018

6. DISCUSSION AND CONCLUSION

Based on Figures 5 and 6, it can be easily observed that the horizontal component estimated based on Sentinel-1A/B data only is noisier than the results from Sentinel-1A/B and ALOS-2 together. However, the difference is very small, and it is hard to judge based on visual interpretation. However, the RMSEs calculated for five CRs presented in Table 3 clearly show that 2D decomposition together with ALOS-2 data allows achieving the best accuracy.

For a better investigation of the effect of ALOS-2 data utilization, the histograms for the horizontal and east-west deformation components are presented. Figure 7 represent for vertical (Fig.7a) and east-west (Fig. 7b) deformation maps for the Sentinel-1A/B variant (orange) and the Sentinel-1A/B and ALOS-2 variant (blue). It can be observed that the histograms from Sentinel-1A/B and ALOS-2 are more similar to the Gaussian one when compare with the solution of Sentinel-1 data only (orange color). Moreover, in Figure 7, it can be observed that some extra bulge is present in the histogram created from Sentinel-1A/B solution only for the vertical as well as horizontal deformation components (orange). After the utilization of ALOS-2 this effect has been removed (Fig.7b) or minimized (Fig.7a).

In this point, it is also worth to mention that we utilized only five ALOS-2 scenes due to the limited availability of ALOS-2 data distributed in the framework of the JAXA Research Agreement. These scenes have been captured with different revisiting times, usually of two or three months. Therefore, it is foreseen that utilization of a bigger number of ALOS-2 scenes with a regular revisiting time of this mission equal to 46 days will bring more benefits. Also, due to the longer wavelength of ALOS-2 data, it is important to minimize atmospheric artefacts since longer wavelengths SAR sensors (L-band; P-band) are more prone mostly to ionospheric artefact when compared with shorter wavelength (X-band) (Gomba, et al., 2015).

Considering these various findings, in future work, we will try to incorporate in our solution more ALOS-2 scenes captured in the framework of the EPOS-PL+ project which is the continuation of the previous EPOS-PL project, and to try better estimate the horizontal deformation component. Even though the RMSE of the east-west horizontal movement is 18mm, this accuracy evaluation has been made for only five measurements points

located on CRs. As is widely known, the accuracy of the interferometric processing is not constant and is changing very quickly across the investigated area. Therefore, in future work we will also try to increase the number of ground truth measurements and incorporate estimation of the atmospheric artefacts.

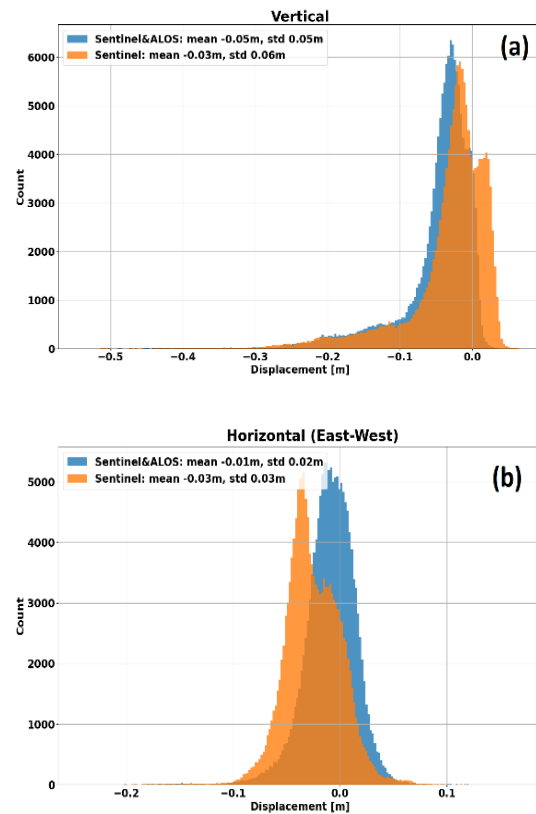


Figure 7. Cumulative deformation from DInSAR estimated for Sentinel-1A/B data only (orange) and for Sentinel-1A/B and ALOS-2 integrated approach (blue) for vertical (a) and horizontal (east-west) component (b)

ACKNOWLEDGEMENTS

The research infrastructure which has been used for computation purposes was created within the project EPOS-PL project - European Plate Observing System - POIR.04.02.00-14-A003/16 and and EPOS-PL+ - POIR.04.02.00-00-C005/19-00 funded by the Operational Programme Smart Growth 2014–2020, Priority IV: Increasing the research potential, Action 4.2: Development of modern research infrastructure of the science sector and co-financed by the European Regional Development Fund. The authors are also very grateful to JAXA for providing the ALOS-2 dataset within the sixth collaborative research agreement (ER2A2N206). Kamila Pawluszek-Filipiak is supported by the Ministry of Science under the scholarship for the best young scientists (SMN/16/1429/2020). The authors are also grateful to Tomasz Hadaś, Krzysztof Sośnica for field campaigns organization and to Krzysztof Stasch and UPWr Master students, who carry out field measurements.

REFERENCES

- Crosetto, M., Monserrat, O., Cuevas-González, M., Devanthery, N., & Crippa, B. (2016). Persistent scatterer interferometry: A review. *ISPRS Journal of Photogrammetry and Remote Sensing*, 115, 78-89. Doi: [10.1016/j.isprsjprs.2015.10.011](https://doi.org/10.1016/j.isprsjprs.2015.10.011)
- Dach, R., Schaer, S., Arnold, D., Prange, L., Sidorov, D., Sušnik, A., ... & Jäggi, A. (2016). CODE final product series for the IGS. Published by Astronomical Institute, University of Bern.
- Ferretti, A., Prati, C., and Rocca, F. 2000. Nonlinear subsidence rate estimation using permanent scatterers in differential SAR interferometry, *IEEE Transactions on geoscience and remote sensing*, 38, 2202–2212. Doi: [10.1109/36.868878](https://doi.org/10.1109/36.868878)
- Ferretti, A., Prati, C., and Rocca, F. 2001. Permanent scatterers in SAR interferometry. *IEEE Transactions on geoscience and remote sensing*, 39(1), 8-20. Doi: [10.1109/36.898661](https://doi.org/10.1109/36.898661)
- Fuhrmann, T., & Garthwaite, M. C. (2019). Resolving three-dimensional surface motion with InSAR: Constraints from multi-geometry data fusion. *Remote Sensing*, 11(3), 241. Doi: [10.3390/rs11030241](https://doi.org/10.3390/rs11030241)
- Gernhardt, S., & Bamler, R. (2012). Deformation monitoring of single buildings using meter-resolution SAR data in PSI. *ISPRS journal of photogrammetry and remote sensing*, 73, 68-79. Doi: [10.1016/j.isprsjprs.2012.06.009](https://doi.org/10.1016/j.isprsjprs.2012.06.009)
- Gomba, G., Parizzi, A., De Zan, F., Eineder, M., & Bamler, R. (2015). Toward operational compensation of ionospheric effects in SAR interferograms: The split-spectrum method. *IEEE Transactions on Geoscience and Remote Sensing*, 54(3), 1446-1461. Doi: [10.1109/TGRS.2015.2481079](https://doi.org/10.1109/TGRS.2015.2481079)
- Hanssen, R. F. (2001). Radar interferometry: data interpretation and error analysis (Vol. 2). Springer Science & Business Media.
- Ilieva, M., Polanin, P., Borkowski, A., Gruchlik, P., Smolak, K., Kowalski, A., and Rohm, W. 2019. Mining Deformation Life Cycle in the Light of InSAR and Deformation Models. *Remote Sensing*, 11(7), 745. Doi: [10.3390/rs11070745](https://doi.org/10.3390/rs11070745)
- Mutke, G., Kotyrba, A., Lurka, A., Olszewska, D., Dykowski, P., Borkowski, A., ... and Barański, A. 2019. Upper Silesian Geophysical Observation System A unit of the EPOS project. *Journal of Sustainable Mining*, 18(4), 198-207. Doi: [10.1016/j.jsm.2019.07.005](https://doi.org/10.1016/j.jsm.2019.07.005)
- Pawluszek-Filipiak, K., & Borkowski, A. (2020). Comparison of PSI and DInSAR approach for the subsidence monitoring caused by coal mining exploitation. The International Archives of Photogrammetry, Remote Sensing and Spatial Information Sciences, 43, 333-337. DOI: [10.5194/isprs-archives-XLIII-B3-2020-333-2020](https://doi.org/10.5194/isprs-archives-XLIII-B3-2020-333-2020)
- Pawluszek-Filipiak, K., & Borkowski, A. (2021). Monitoring mining-induced subsidence by integrating differential radar interferometry and persistent scatterer techniques. *European Journal of Remote Sensing*, 54(sup1), doi: [10.1080/22797254.2020.1759455](https://doi.org/10.1080/22797254.2020.1759455)
- Pawluszek-Filipiak, K., Wielgocka, N., Lewandowski, T., & Tondaś, D. (2021). Assessing the application of GACOS atmospheric correction for DInSAR-based mining deformation monitoring by using Sentinel-1 data in Upper Silesian Coal Basin in Poland. *Geodesy and Cartography*, Vol. 70, no. 2, article no. e10, 2021. DOI: <https://doi.org/10.24425/gac.2021.136685>
- Pepe, A., Solaro, G., & Dema, C. (2012). A minimum curvature combination method for the generation of multi-platform DInSAR deformation time-series. *Geophysical Journal International*, 191, 1095-1108.
- Samsonov, S., Dille, A., Dewitte, O., Kervyn, F., & d'Oreye, N. (2020). Satellite interferometry for mapping surface deformation time series in one, two and three dimensions: A new method illustrated on a slow-moving landslide. *Engineering Geology*, 266, 105471 Doi: [10.1016/j.enggeo.2019.105471](https://doi.org/10.1016/j.enggeo.2019.105471)
- Sun, Q., Hu, J., Zhang, L., & Ding, X. (2016). Towards slow-moving landslide monitoring by integrating multi-sensor InSAR time series datasets: The Zhouqu case study, China. *Remote Sensing*, 8(11), 908. Doi: [10.3390/rs8110908](https://doi.org/10.3390/rs8110908)
- Wang, Z., Yu, S., Tao, Q., Liu, G., Hao, H., Wang, K., & Zhou, C. (2018). A method of monitoring three-dimensional ground displacement in mining areas by integrating multiple InSAR methods. *International journal of remote sensing*, 39(4), 1199-1219. doi: [10.1080/01431161.2017.1399473](https://doi.org/10.1080/01431161.2017.1399473)
- Wnuk, K.; Zhou, W.; Gutierrez, M. Mapping Urban Excavation Induced Deformation in 3D via Multiplatform InSAR Time-Series. *Remote Sens.* 2021, 13, 4748. Doi: [10.3390/rs13234748](https://doi.org/10.3390/rs13234748)
- Yang, Z., Li, Z., Zhu, J., Feng, G., Wang, Q., Hu, J., & Wang, C. (2018). Deriving time-series three-dimensional displacements of mining areas from a single-geometry InSAR dataset. *Journal of Geodesy*, 92(5), 529-544. Doi: [10.1007/s00190-017-1079-x](https://doi.org/10.1007/s00190-017-1079-x)
- Zhang, L., Cai, X., Wang, Y., Wei, W., Liu, B., Jia, S., ... & Wei, Z. (2020). Long-term ground multi-level deformation fusion and analysis based on a combination of deformation prior fusion model and OTD-InSAR for longwall mining activity. *Measurement*, 161. Doi: [10.1016/j.measurement.2020.107911](https://doi.org/10.1016/j.measurement.2020.107911)